Molecular Biology of the Cell
Vol. 17, 1971–1984, April 2006

A Genetic Dissection of Aip1p's Interactions Leads to a Model for Aip1p–Cofilin Cooperative Activities[D]

Michael G. Clark,* Joseph Teply,† Brian K. Haarer,* Susan C. Viggiano,* David Sept,† and David C. Amberg*

*Department of Biochemistry and Molecular Biology, SUNY Upstate Medical University, Syracuse, NY 13210; and †Department of Biomedical Engineering and Center for Computational Biology, Washington University, St. Louis, MO 63130

Submitted October 14, 2005; Revised December 27, 2005; Accepted January 6, 2006
Monitoring Editor: Thomas Pollard

Actin interacting protein 1 (Aip1p) and cofilin cooperate to disassemble actin filaments in vitro and are thought to promote rapid turnover of actin networks in vivo. The precise method by which Aip1p participates in these activities has not been defined, although severing and barbed-end capping of actin filaments have been proposed. To better describe the mechanisms and biological consequences of Aip1p activities, we undertook an extensive mutagenesis of *AIP1* aimed at disrupting and mapping Aip1p interactions. Site-directed mutagenesis suggested that Aip1p has two actin binding sites, the primary actin binding site lies on the edge of its N-terminal β-propeller and a secondary actin binding site lies in a comparable location on its C-terminal β-propeller. Random mutagenesis followed by screening for separation of function mutants led to the identification of several mutants specifically defective for interacting with cofilin but still able to interact with actin. These mutants suggested that cofilin binds across the cleft between the two propeller domains, leaving the actin binding sites exposed and flanking the cofilin binding site. Biochemical, genetic, and cell biological analyses confirmed that the actin binding- and cofilin binding-specific mutants are functionally defective, whereas the genetic analyses further suggested a role for Aip1p in an early, internalization step of endocytosis. A complementary, unbiased molecular modeling approach was used to derive putative structures for the Aip1p–cofilin complex, the most stable of which is completely consistent with the mutagenesis data. We theorize that Aip1p-severing activity may involve simultaneous binding to two actin subunits with cofilin wedged between the two actin binding sites of the N- and C-terminal propeller domains.

INTRODUCTION

Actin cytoskeleton dynamics requires precise and adaptable modes of regulation to carry out a multitude of essential cellular activities. Throughout the cell, actin interacting proteins work cooperatively to conduct cytoskeletal functions with a complexity that is only beginning to be understood. Many cellular processes, including those as basic as cell division and growth, demand the rapid turnover of actin networks, of which filament disassembly is a major rate-limiting factor. Actin interacting protein 1 (Aip1p) and cofilin are two actin binding proteins that function in concert to promote the rapid disassembly of actin filaments. Biochemical assays show that cofilin promotes depolymerization of actin filaments by accelerating pointed-end filament disassembly (Carlier *et al*., 1997; Lappalainen and Drubin, 1997) and by a severing activity that is very weak at physiological pH (Maciver *et al*., 1991; Ichetovkin *et al*., 2000). Aip1p dramatically enhances the depolymerization activity of cofilin-decorated actin filaments and is suspected to do so by assisting cofilin-induced severing and/or by capping the barbed ends of actin filaments (Okada *et al*., 1999; Rodal *et al*., 1999; Okada *et al*., 2002; Balcer *et al*., 2003; Mohri *et al*., 2004; Ono *et al*., 2004).

In *Saccharomyces cerevisiae*, an *aip1* null mutant strain is viable and has subtle defects in actin organization, including apparent excessive actin assembly in actin cortical patches (Rodal *et al*., 1999). However, synthetic lethal interactions occur when an *AIP1* deletion is combined with specific cofilin alleles (Iida and Yahara, 1999; Rodal *et al*., 1999), confirming a biological role for Aip1p in yeast. Furthermore, partial mislocalization of cofilin from cortical patches to actin cables has been observed in an *aip1*Δ yeast strain (Rodal *et al*., 1999). Aip1p is evolutionarily conserved and has been identified in a number of organisms as an important regulator of cytoskeletal dynamics. *Xenopus* Aip1p (XAip1) localizes to the cell cortex, cytoplasm, and nuclei (Okada *et al*., 1999). RNA interference (RNAi) inhibition of Aip1p in *Drosophila* S2 cells leads to accumulation of cortical F-actin and cell surface morphology defects (Rogers *et al*., 2003). In *Caenorhabditis elegans*, the loss of Aip1p (UNC-78) results in disorganized assembly of actin filaments in body wall muscle (Ono, 2001). A *Dictyostelium* null mutant shows impairments in chromosome segregation reliability, motility, endocytosis, and cytokinesis (Konzok *et al*., 1999; Gerisch *et al*., 2004). Last, in *Arabidopsis*, RNAi-induced reductions in Aip1p expression correlate with reduced leaf and plant size that at the lowest expression levels render the plant inviable (Ketelaar *et al*., 2004). This broad range of phenotypic defects

This article was published online ahead of print in *MBC in Press* (http://www.molbiolcell.org/cgi/doi/10.1091/mbc.E05–10–0956) on January 18, 2006.

[D] The online version of this article contains supplemental material at *MBC Online* (http://www.molbiolcell.org).

Address correspondence to: David C. Amberg (ambergd@upstate.edu).

suggests a central role for Aip1p in actin network organization and dynamics.

Aip1p consists of two contiguous seven-bladed β-propeller domains, each made up of seven WD-repeats (Figure 1A; Voegtli *et al*., 2003). The propellers are positioned at an angle to one another such that one surface of the molecule is concave, whereas the other is convex, and we refer to these as the front and back of the molecule, respectively. Aip1p was first identified in *S. cerevisiae* through its two-hybrid interaction with actin (Amberg *et al*., 1995). Subsequent two-hybrid analysis identified a physical interaction between Aip1p and cofilin (Rodal *et al*., 1999), although biochemical and two-hybrid analyses suggested that the interaction is stabilized by actin (Rodal *et al*., 1999). Aip1p was also found to be functionally related to cofilin because of its ability to suppress a *cof1* temperature-sensitive mutant upon overexpression (Iida and Yahara, 1999). Aip1p increases filament disassembly at low stoichiometry, but this is dependent upon cofilin decoration of the filament and is optimal when the ratio of cofilin to actin is 1:1 (Rodal *et al*., 1999). Binding of Aip1p to cofilin-decorated actin filaments occurs laterally along the length of the filament and at filament ends (Okada *et al*., 1999). This "end-capping" of the actin filament has been suggested to assist cofilin by preventing elongation and reannealing of severed filaments (Okada *et al*., 1999). However, tethered actin filament assays conducted in the presence of cofilin, Aip1p, and filament-capping proteins favor an alternate proposal first presented by Rodal *et al*. (1999) in which Aip1p enhances the weak severing ability of cofilin (Ono *et al*., 2004). Therefore, additional evidence is needed to elucidate the mechanism of Aip1p's ability to enhance filament disassembly, in particular, the contributions of severing versus capping.

To understand how Aip1p binding may alter the actin filament, there is a need to further define the molecular interactions within the Aip1p–cofilin–actin complex. Electron cryomicroscopy of cofilin-decorated filaments revealed that cofilin simultaneously binds two longitudinally adjacent actin monomers (McGough *et al*., 1997). The cofilin interaction sites on actin are predicted to be between domains 1 and 3 for the upper actin subunit and on domains 2 and 1 of the lower subunit (McGough *et al*., 1997). Yeast two-hybrid analyses confirm that charged amino acid residues in subdomain 3 of actin are essential for the cofilin interaction and also indicate that Aip1p binds subdomain 4 of actin, in a cofilin-dependent manner (Amberg *et al*., 1995; Rodal *et al*., 1999). This suggests that cofilin binding, by altering actin filament structure, creates a conformational change conducive to the Aip1p interaction. Cofilin contains two actin binding sites: the first site is essential for all actin interactions and is predicted to bind domains 1 and 3 of actin, whereas the second is essential for the F-actin interactions and is predicted to bind domains 1 and 2 of actin (Lappalainen and Drubin, 1997).

On cofilin decoration of F-actin, the longitudinal contacts between subdomains 1 and 2 of adjacent actin monomers are destabilized (Bobkov *et al*., 2002; Galkin *et al*., 2003). Similar loss of longitudinal contacts have been observed at the pointed ends of undecorated actin filaments, suggesting that cofilin binding maintains a preexisting destabilized conformation of the actin filament (Galkin *et al*., 2003). This is frequently associated with a 4–5°/subunit reduction in the actin filament twist (McGough *et al*., 1997). We hypothesize that this conformation may be optimal for Aip1p binding along the length of the filament, further destabilizing filaments through an intensified structural distortion that leads to enhanced filament breakage. After filament cleavage,

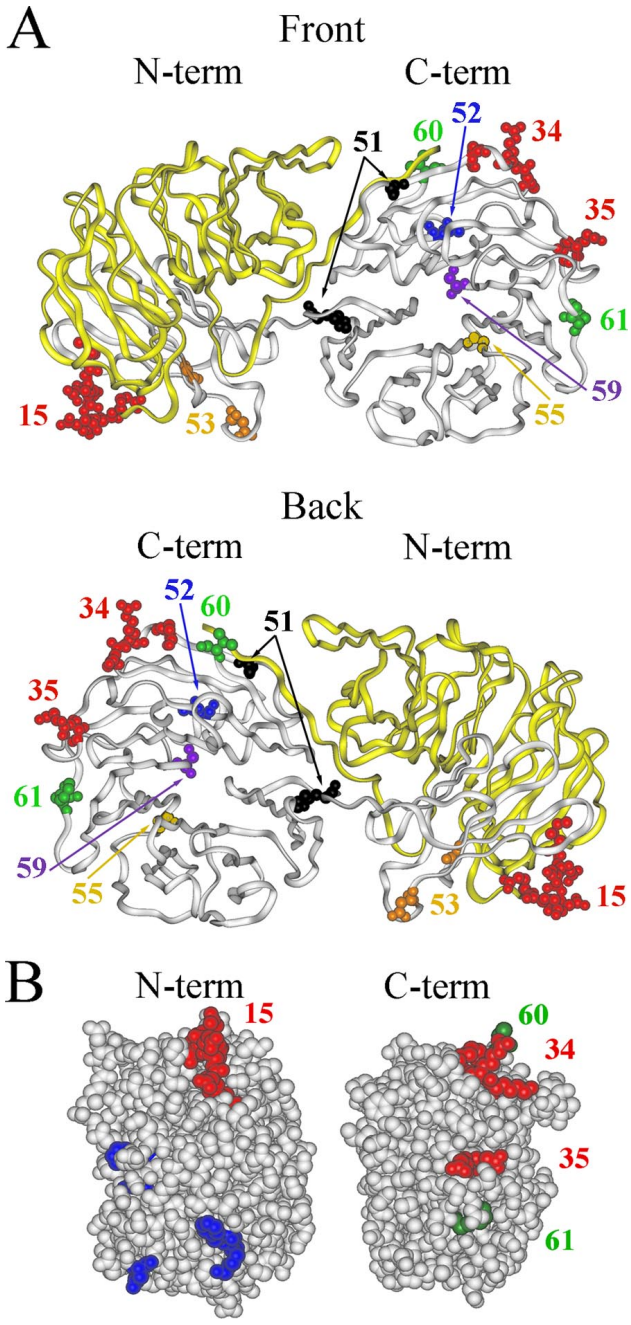

Figure 1. Aip1p mutagenesis reveals actin and cofilin binding footprints on Aip1p. (A) Aip1p is shown from a front (top) and back (bottom) view with residues changed by *aip1* mutant alleles highlighted. Residues involved in the actin interaction are highlighted in red. The region expressed by the *aip1-56* truncation mutant, which interacts with actin but not cofilin, is colored in yellow. Cofilin-specific alleles are shown in orange, black, blue, purple, and brown. (B) Sides views of the Aip1p N-terminal (left) and C-terminal (right) propellers depict analogous actin binding domains. Red residues represent loss-of-function cluster charged-to-alanine mutations involved in the actin interaction. Green residues represent randomly selected gain-in-function mutants that apparently increased the Aip1p–actin two-hybrid interaction. Blue residues represent the *S. cerevisiae* equivalents of site-directed mutants generated in *C. elegans AIP1* (UNC-78) that are defective for actin filament disassembly in vitro (Mohri *et al*., 2004).

Aip1p may remain bound to the newly formed filament barbed end, where it could potentially assist in barbed-end regulation.

To further unravel the molecular details of interactions within the Aip1p–cofilin–actin complex, we have undertaken a genetic dissection of *AIP1* aimed at defining functional sites on Aip1p. This analysis confirmed the presence of a strong actin binding site on the N-terminal propeller of Aip1p (Mohri *et al*., 2004) but suggested an additional site of contact for actin on the analogous region of the C-terminal propeller. Separation-of-function mutants define a possible site of interaction for cofilin between the two actin binding sites of Aip1p bridging the two β-propeller domains. These data are completely consistent with an independently derived molecular model for the Aip1p–cofilin interaction. In addition, biochemical, genetic, and cytological approaches were used to further define the role of Aip1p within *S. cerevisiae*, while also attempting to address the filament severing versus filament capping debate. Our data link Aip1p to a discrete step in the process of endocytosis and for the first time indicate a physiological role for Aip1p in *S. cerevisiae*.

MATERIALS AND METHODS

Yeast Two-Hybrid Analysis of Site-directed and Random aip1 Mutants

Plasmid pAIP6 encoding a fusion of the *GAL4* activation domain (AD) to *AIP1* (Amberg *et al*., 1995) in vector pACT (Durfee *et al*., 1993) was the template in PCR reactions using Advantage DNA Polymerase (Clontech, Mountain View, CA). Site-directed mutants for cluster-charge-to-alanine scan alleles were created by overlap extension fusion PCR with external primers 2H1 (5′-TGATGAAGATACCCCACC-3′) and 2H5 (5′-ACAGTTGAAGTGAACTTGCG-3′) and internal primers specific to the mutant allele. The resulting PCR product was cotransformed with double-digested (BamHI and EcoRI) plasmid pACTII (gift of S. Elledge, Howard Hughes Medical Institute, Center for Genetics and Genomics, Boston, MA) by lithium acetate (Rose *et al*., 1989) into yeast strain Y187 (Table 1; Durfee *et al*., 1993), and the gap repair transformants were selected on SC-Leu plate medium. The transformants were analyzed for their abilities to interact with actin and cofilin by yeast two-hybrid analysis (Fields and Song, 1989). Briefly, Y187 cells carrying mutant *aip1*-AD fusion plasmids were spotted on SC-Leu and allowed to grow overnight. These were then replica plated to duplicate YPD plates, which were overlaid with a lawn of yeast strain Y190 transformed with plasmid pDAb7 encoding a fusion of *ACT1* to the *GAL4* DNA binding domain (Amberg *et al*., 1995) or plasmid pTY1 encoding a fusion of *COF1* to the *GAL4* DNA binding domain. The cells were allowed to mate for 1 d after which diploids were selected on SC media lacking tryptophan and leucine. The diploids were then replica plated to SD medium plus 10 μg/ml adenine and 25, 50, or 100 mM 3,5-aminotriazole. All mutants were rescued and amplified in *Escherichia coli* by standard methods (Rose *et al*., 1989).

Random PCR mutagenesis used a similar method, except Taq polymerase was substituted. Successful transformants were screened for an ability to interact with actin, but not cofilin, or vice versa. Mutants showing such a defect were rescued, retested to confirm their specific defects, and submitted for sequencing. Images of *aip1p* mutants were generated using Insight II Version 2000 (Molecular Simulations, San Diego, CA). Coordinates for Aip1p were retrieved from the Collaboratory for Structural Bioinformatics Protein Data Bank (PDB file 1PI6).

Genomic Integration of aip1 Mutants

To generate strains carrying mutated *aip1* genes, *aip1*-x:G418^r cassettes were created by cloning appropriate mutation-containing *aip1* fragments out of the two-hybrid vectors and into the plasmid pMC60 and then excising the *aip1*-x:G418^r cassettes with SalI and KpnI; pMC60 contains the *aip1*-x:G418^r cassette cloned into pBluescript II KS (+/−) (Stratagene, La Jolla, CA). An *aip1*-x:G418^r cassette was inserted into the *aip1*Δ::URA3 genomic locus of diploid strain LGY2xLGY3 by homologous recombination. Successful transformants were selected on YPD + G418 media. Strains were confirmed by sequencing PCR products generated using external primers LGo-Aip1-1 (5′-AATACTAGCTATTGCTTTCCG-3′) and MCo-Aip1-130 (5′-AGTCTTTTCCTTACCCAT-3′) on genomic DNA templates.

Synthetic Sick/Lethal Testing of aip1 Mutants

For *aip1* × *cof1-4* analyses, *aip1* mutant strains (*MAT* **a** *aip1-x:G418^r ura3-52 trp1*Δ) were crossed to DDY1253. Diploids were selected on SC-leu + G418 media, sporulated for 4 to 6 d at 25°C, dissected, and analyzed for synthetic viability or growth defects.

For the *aip1*Δ × endocytosis-related gene deletion screen, yeast strain MCY60 was hand-crossed against 86 different gene deletion mutants from the EUROSCARF collection (*MAT* **a** *gene*Δ*::G418^r ura3-52 leu2*Δ*1 met15*Δ *his3*Δ). Diploids were selected on YPD + G418 + Nat^r and then sporulated for 4 to 6 d at 25°C and dissected. Dissected tetrads were plated onto YPD, allowed to grow overnight at 30°C, and then replica plated to YPD + G418 (30°C) and YPD + Nat (30°C), to identify colonies in which both deletion alleles cosegregated. When double deletion mutant colonies remained viable, they were struck on YPD for single colonies and plated at 30 and 37°C to inspect for growth defects.

EUROSCARF deletion alleles that showed synthetic defects with an *aip*Δ were also tested against our array of *aip1* mutant strains (*MAT* **a** *aip1-x:G418^r ura3-52 trp1*Δ). Because both mutations were marked with *G418^r*, PD versus NPD tetrads were used to identify synthetic growth defects at 30 and 37°C.

Yeast Immunofluorescence

Immunofluorescence was performed by standard protocols using a methanol/acetone fixation (Amberg *et al*., 2005). Affinity-purified anti-Aip1p anti-

Table 1. *S. cerevisiae* strains

Name	Genotype	Source
FY23x86	*MAT***a**/α *ura3-52/ura3-52 leu2*Δ*1/leu2*Δ*1 trp1*Δ*63/TRP1 HIS3/his3*Δ*200*	Rodal *et al*. (1999)
Y187	*MAT*α *gal4 gal80 his3 trp1-901 ade2-101 ura3-52 leu2-3,112 GAL—lacZ*	Bai and Elledge (1996)
Y190	*MAT***a** *gal4 gal80 his3 trp1-901 ade2-101 ura3-52 leu2-3,112 URA3::GAL—lacZ LYS2::GAL—HIS3cyh^r*	Bai and Elledge (1996)
LGY2x3	*MAT***a**/α *aip1*Δ*::URA3/aip1*Δ*::URA3 ura3-52/ura3-52 leu2*Δ*1/leu2*Δ*1 trp1D63/TRP1 HIS3/his3*Δ*200*	Rodal *et al*. (1999)
DDY1253	*MAT*α *ura3-52 his3*Δ*200 lys2-801 cof1-4*	Lappalainen *et al*. (1997)
DDY1264	*MAT*α *ura3-52 his3*Δ*200 lys2-801 cof1-19*	Lappalainen *et al*. (1997)
MCY9	*MAT***a** *aip1-15:G418^r ura3-52 leu2*Δ*1 his3*Δ*200*	
MCY10	*MAT*α *aip1-15:G418^r ura3-52 leu2*Δ*1 trp1*Δ*63*	
MCY13	*MAT***a** *aip1-55:G418^r ura3-52 leu2*Δ*1 his3*Δ*200*	
MCY14	*MAT*α *aip1-55:G418^r ura3-52 leu2*Δ*1 trp1*Δ*63*	
MCY17	*MAT***a** *aip1-59:G418^r ura3-52 leu2*Δ*1 trp1*Δ*63*	
MCY18	*MAT*α *aip1-59:G418^r ura3-52 leu2*Δ*1 his3*Δ*200*	
MCY21	*MAT***a** *aip1-34/35:G418^r ura3-52 leu2*Δ*1 trp1*Δ*63*	
MCY22	*MAT*α *aip1-34/35:G418^r ura3-52 leu2*Δ*1 his3*Δ*200*	
MCY25	*MAT***a** *aip1-60:G418^r ura3-52 leu2*Δ*1 trp1*Δ*63*	
MCY26	*MAT*α *aip1-60:G418^r ura3-52 leu2*Δ*1 his3*Δ*200*	
MCY27	*MAT***a** *cof1-19:LEU2 aip1-60:G418^r ura3-52 leu2*Δ*1 trp1*Δ*63*	
MCY60	*MAT*α *aip1*Δ*::NAT ura3*Δ*0 leu*Δ*0 his3*Δ*1 lys2*Δ*0 mfa1*Δ*::P$_{MFA1}$-spHIS5*	

body (primary) was used at a dilution of 1:100. Affinity-purified rabbit anti-cofilin antibody (primary) was used at 1:100 (Rodal *et al*., 1999). Fluorescein isothiocyanate-conjugated goat anti-rabbit IgG (Cappel, Costa Mesa, CA; ICN Biochemicals) was used at 1:1000.

Rhodamine-Phalloidin Staining

Staining of the actin cytoskeleton was performed using a standard protocol (Amberg *et al*., 2005). Briefly, a yeast cell culture grown to 2×10^7 was subjected to incubation with electron microscopy-grade formaldehyde at a final concentration of 4%, washed with phosphate-buffered saline (PBS), and treated with rhodamine-labeled phalloidin (1:10 dilution of 6.6 μM in methanol). After washing again with PBS, cells were suspended in mounting solution and viewed by fluorescence microscopy.

Protein Purification

Yeast actin was purified by a modified DNaseI affinity purification procedure (Kron *et al*., 1992). Briefly, 200 mg of DNase I (Roche Diagnostics, Indianapolis, IN) was coupled to 5 g of swelled Sepharose 4B (Sigma-Aldrich, St. Louis, MO) according to the manufacturer's instructions. Then, 3 ml of DNase I-Sepharose was loaded into a 2.5 × 10-cm Econo-column (Bio-Rad, Hercules, CA), the column was washed with: 15 ml of 10% formamide in G-buffer (10 mM Tris, pH 7.5, 0.5 mM ATP, 0.2 mM dithiothreitol [DTT], and 0.2 mM $CaCl_2$), 15 ml of G-buffer + 0.2 M NH_4Cl, and 15 ml of G-buffer. Four liters of yeast strain FY23 × 86 was grown to a density of ~2×10^7 cells/ml, pelleted in four tubes, and each resuspended in 40 ml of G-buffer (+ATP, DTT, phenylmethylsulfonyl fluoride, and Calbiochem protease inhibitor cocktail). Each was passed once through a French Press set at 1200 psig. The lysate was clarified in a Beckman JA-20 rotor at 12,000 rpm for 30 min at 4°C and then in a Beckman Ti50.2 rotor at 40,000 rpm for 120 min at 4°C. The supernatant was loaded in equal volumes onto two DNase I columns at a flow rate of ~1–2 ml/min. Each column was washed with 15 ml of G-buffer + 10% deionized formamide, 14 ml of G-buffer + 0.2 M NH_4Cl, and 15 ml of G-buffer. The actin was eluted with 15 ml of G-buffer + 50% deionized formamide. Contaminating formamide was removed by dialyzing overnight in 1 liter of G-buffer (0.05 μM ATP). Samples were concentrated in a Micron-10 device (Amicon, Billerica, MA), clarified by ultracentrifugation in a Beckman TLA100 rotor at 90,000 rpm for 20 min at 4°C, snap frozen, and stored at −80°C until use. Bradford assays were used to determine protein concentration.

Yeast cofilin was expressed in *E. coli* DH5α cells as a glutathione *S*-transferase (GST) fusion protein under the control of the P_{lac} promoter. GST-cofilin was purified as described previously (Lappalainen and Drubin, 1997) but with the following alterations. Cells were grown to stationary phase in 1 liter of Luria broth + ampicillin. PBS was substituted with Tris-buffered saline (TBS) (50 mM Tris, pH 7.5, and 100 mM NaCl) in all relevant steps. Before binding to glutathione-agarose resin, Triton X-100 was mixed with the lysate to a 1% final concentration and then was spun in a Beckman centrifuge using a JA-20 rotor at 10,000 rpm for 20 min. The supernatant was extracted, added to 1.5 ml of a 50% resin slurry, and rocked for 90 min at room temperature. After washing 4 × 10 ml of ice-cold TBS, thrombin was added to the beads (3 ml of TBS, 10.4 μl of 0.5 M $CaCl_2$, and 50 μl of thrombin at 1 U/μl) and incubated at room temperature for 3 h. After cleavage, the supernatant was collected and the resin was washed with 2 × 2 ml of TBS, washes were added to the supernatant. This was dialyzed overnight against 50 mM Tris, pH 7.5, at 4°C. Samples were further purified by fast-performance liquid chromatography (Bio-Rad) on a UNO-Q1 column and washed at 1 ml/min with 50 mM Tris, pH 7.5 and then eluted with a linear KCl gradient (100–400 mM) in 50 mM Tris, pH 7.5. Peak fractions were dialyzed overnight against 10 mM Tris, pH 7.5, and 50 mM NaCl for 5 h at 4°C, concentrated (Microcon YM-10 columns, Millipore, Bedford, MA), confirmed by Western assay, and stored at −80°C.

Yeast Aip1p was expressed in yeast cells as a GST fusion protein under the control of a galactose-inducible promoter [pEG(KT)]. Cells were inoculated into 1 liter of SC-Ura-Leu + 3% glycerol + 1% EtOH + 0.1% glucose and grown for 20–24 h at 30°C. Galactose was added to a 2% final concentration and induction continued for 10 h. GST-Aip1p purification proceeded as described for GST-cofilin, with the following alterations. Before binding to glutathione-agarose resin, cell lysate (with no Triton X-100) was pelleted in a Beckman centrifuge using a JA-20 rotor at 12 krpm for 30 min. The supernatant was then spun again in a Beckman ultracentrifuge using a 70 Ti rotor at 50,000 rpm for 50 min.

Profilin was purified from yeast strain FY23 × 86 as described previously (Haarer *et al*., 1990). Profilin was stored at 4°C on ice and used within 10 d of purification.

Molecular Docking

The coordinates of Aip1p and cofilin were obtained from the Protein Data Bank (PDB file 1PI6 and 1CFY, respectively). The Aip1p structure was missing a surface loop (544–549) that was first rebuilt using PLOP (Jacobson *et al*., 2004). Using the molecular dynamics package NAMD (Kale, 1999), simulations of both complexes were performed at 300 K using an NPT ensemble with CHARMM27 force-field and explicit solvent (TIP3P water). The molecular dynamics simulations were each comprised of energy minimization, followed by heating to 300 K at intervals of 75 K, equilibration for 500 ps, and finally a production run of 5 ns for Aip1p and 10 ns for cofilin. Representative conformations of each structure were extracted from the trajectory for subsequent use in molecular docking studies. Because both proteins are held rigid during the docking simulation, this step allows us to capture some of the backbone and side chain fluctuations in the proteins. Because cofilin is the smaller protein and exhibited significantly more dynamics than Aip1p, we selected Aip1p structures every 500 ps (total of 10 structures), whereas for cofilin we selected structures every 10 ns, resulting in 1000 conformations. Five docking trajectories were carried out with each combination of Aip1p and cofilin structures using AutoDock 3.0 (Morris *et al*., 1998). The resulting 50,000 docking predictions were clustered based on a root-mean-square deviation of 10 Å, and the structures exhibiting the best clustering were selected as candidate structures. This resulted in a total of six likely docked conformations with one conformation that showed particularly good correspondence with existing mutagenesis data.

RESULTS

Identification of the Actin Interaction Sites on Aip1p

We performed a cluster charged-to-alanine scan (Wertman *et al*., 1992) to introduce surface mutations into *AIP1* to identify potential sites of actin interaction. This technique neutralized charged clusters of amino acid residues on the surface of Aip1p and was thus expected to disrupt points of electrostatic interaction between Aip1p and its binding partners (actin and cofilin). Each of 34 *aip1* mutant alleles (*aip1-1* to *aip1-33*) was tested against actin by yeast two-hybrid analysis (Table 2). Just one allele, *aip1-15*, showed a defect in actin binding, and this was only partial (Figure 2A). *aip1-15*

Table 2. *AIP1* charge-to-alanine scan alleles

Allele	Amino acid changes
1	K7A, E8A
2	Q17A, R18A, N19A
3	D47A, D48A, D50A
4	D85A, E86A, K89A
5	D98A, K99A, E100A, N102A
6	K109A, E111A, Q113A
7	E127A, R129A, R130A
8	E136A, R138A, D139A, N140A
9	N151A, E155A
10	K169A, Q170A, R172A
11	Q161A, R162A
12	K194A
13	D228A, R229A, K230A
14	D235A, K237A
15	I245A, E246A, D247A, D248A, Q249A, E250A
16	D263A, Q265A, K266A
17	D293A, K294A, Q295A, Q296A
18	N299A, Q300A, Q301A
19	D329A, E330A, K333A
20	N339A, K340A
21	D356A, R358A
22	K285A, Q288A, K289A
23	Q369A, D370A
24	K382A, Q384A, E385A
25	N415A, N416A, D417A
26	E464A, E465A, N467A
27	D516A, Q518A, R520A, E521A
28A	E543A, K544A
28B	N547A, E548A, E549A, E550A
29	I551A, E552A, E553A, D554A
30	D562A, N564A
31	K575A, K578A
32	N588A, N589A
33	K608A, R609A, N611A
34	K571A, R572A, K575A
35	D516A, E521A

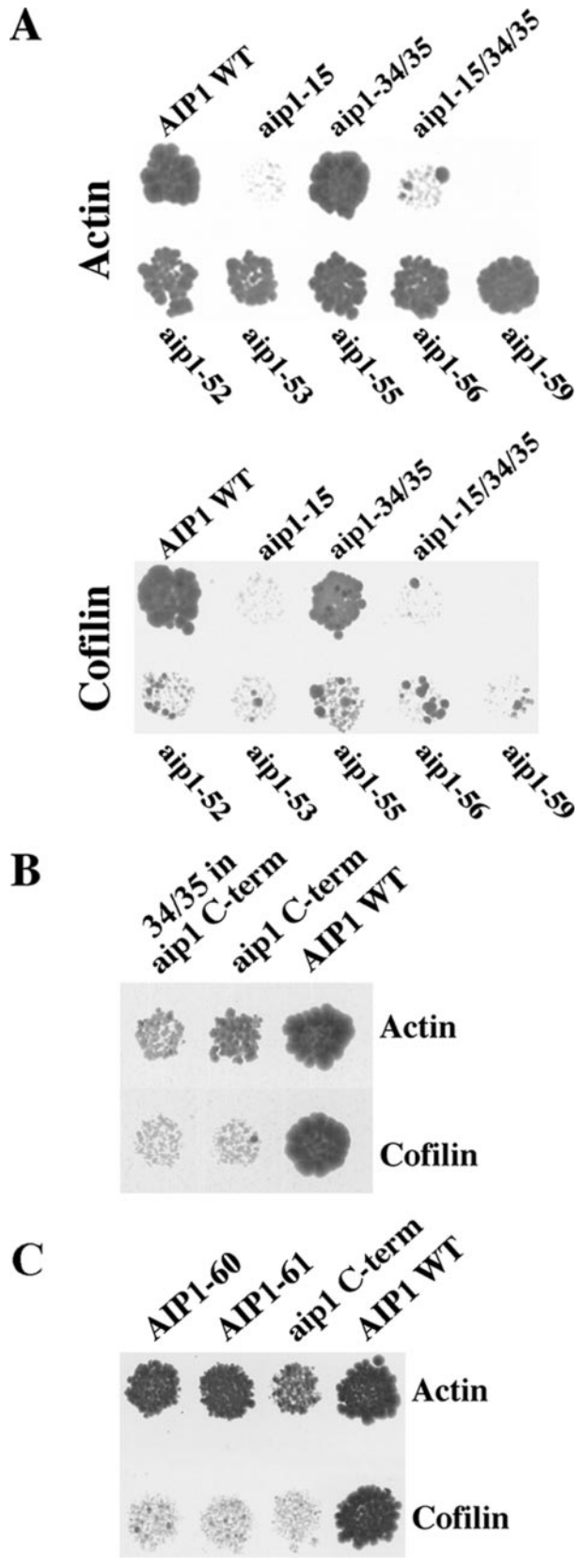

Figure 2. Two-hybrid analysis of *aip1* mutants. (A) Yeast two-hybrid interactions between mutants of Aip1p and actin (top) or cofilin (bottom) were measured based on activation of expression of the *HIS3* reporter (growth on minimal media containing 100 mM 3-AT [top] and 50 mM 3-AT [bottom]). (B) The C-terminal propeller of aip1p (aip1 C-term) interacts by yeast two-hybrid with actin but not with cofilin (10 mM 3-AT). This interaction is severely impaired by addition of the *aip1-34/35* mutations. (C) Two spontaneously generated mutants on the aip1 C-term (*aip1-60* and *aip1-61*) increase the two-hybrid interaction with actin.

neutralizes a prominent patch of negatively charged residues (I245A, E246A, D247A, D248A, Q249A, E250A) within blade five of the N-terminal β-propeller (Figure 1A).

The inability of the charged-to-alanine scan to identify mutants that resulted in a complete loss of actin binding suggested either that the actin interacting site is too large to effectively disrupt with the neutralization of a single charged cluster or that more than one actin binding site exists on Aip1p. Taking into consideration the possibility that the double propeller structure of Aip1p could be the result of a gene duplication, we tested the C-terminal β-propeller (residues 337–615) for the ability to interact with actin in the two-hybrid system. As shown in Figure 2B, the C-terminal propeller of Aip1p demonstrates a weak two-hybrid interaction with actin.

Despite low protein sequence homology between the two propellers, we chose to test whether the observed functional homology (actin binding) corresponds to an actin interacting site located within corresponding regions of each propeller. Therefore, two charged clusters that had not been specifically targeted previously were identified at a region of the C-terminal propeller that is located in a structurally and sequentially similar location to the analogous region of the N-terminal propeller where the *aip1-15* mutation is located. Each was converted to a new charged-to-alanine allele. These two alleles, *aip1-34* (K571A, R572A, K575A) and *aip1-35* (D516A, E521A) lie on the sixth and fifth blades, respectively, of the C-terminal propeller (Table 2 and Figure 1, A and B). When tested in the context of full-length Aip1p for a two-hybrid interaction with actin, neither of the mutants alone or in combination showed a defect (Figure 2A). However, when the *aip1-15* mutant was tested in combination with the *aip1-34* and *aip1-35* mutants, the actin interaction was eliminated (Figure 2A). Furthermore, when the *aip1-34* and *aip1-35* mutations were combined in the context of the C-terminal propeller alone (residues 337–615), the weak actin interaction of this domain was markedly impaired (Figure 2B). These data suggest that two analogous actin binding sites are located on Aip1p: one on each β-propeller (Figure 1, A and B).

Confirmation of Two Independent Actin Interaction Sites

Additional mutants have been recovered that strengthen the argument that each of the two propellers contains an actin binding site. In each case, a random mutagenesis technique was implemented. First, the *AIP1* gene was mutated through a PCR reaction in which a low fidelity Taq polymerase was used to incorporate random mutations into the gene. These mutated PCR products were introduced by recombination (Ma *et al.*, 1987) into a two-hybrid DNA activation domain vector and differential interaction screening was used to isolate separation-of-function mutants that had the ability to interact with actin but not cofilin in two-hybrid assays. From this we recovered *aip1-56*, which replaces Trp261 with a stop codon, ending translation of Aip1p ~80% into the N-terminal propeller. Thus, an N-terminal domain was identified that binds actin independent of the C-terminal propeller (Figure 1A in yellow and Figure 2A).

A slightly different strategy was used to confirm the site of actin interaction on the C-terminal propeller. The C-terminal propeller domain (expressing amino acids 337–615), which shows a weak two-hybrid interaction with actin and none with cofilin, was subjected to low-fidelity PCR as described above and screened in the two-hybrid system for gain-in-function mutations that display an apparent increased actin interaction. Two mutants were identified that increased activation of the two-hybrid reporters when tested against actin; sequencing of *aip1-60* and *aip1-61* revealed mutations Glu615Lys and Phe481Leu, respectively. These residues map very close and on either side of the *aip1-34* and *aip1-35* mutations, supporting the presence of an actin interacting site on the C-terminal propeller that is consistent with the location suggested by the two-hybrid results with the *aip1-34* and *aip1-35* mutants (Figures 1, A and B, and 2C; the final two C-terminal amino acid residues of Aip1p were not resolved in this crystal structure, so *aip1-60*, shown at residue 613, is actually closer to *aip1-34* than this illustration suggests).

Differential Interaction Screening Identifies the Cofilin Interaction Site on Aip1p

To identify the cofilin binding site on Aip1p, random mutagenesis and differential interaction screening, as described above, were used to genetically dissect the ability of Aip1p to interact with actin and cofilin by two-hybrid. Mutants were selected based on an ability to interact well with actin at high levels of 3-AT inhibition of the His3p reporter but not with cofilin, even at low levels of 3-AT inhibition. By screening for isolates that did not lose their actin interacting activity, we targeted mutants that presumably maintain sound structural integrity, thus limiting their defects to the cofilin interaction site.

Three separate single mutations were found that were able to separate the actin and cofilin interactions: *aip1-52* (Thr558Pro), *aip1-55* (Gly449Asp), and *aip1-59* (Ser492Leu) (Figures 1A and 2A). These mutations lay toward the center of the C-terminal propeller, between blades 5 and 6, 3 and 4, and 4 and 5, respectively, and suggest the existence of a cofilin interaction site on the front surface of the C-terminal propeller. A fourth mutant allele of the same phenotype, *aip1-51*, includes a combination of two mutations, H338P and A579T (our unpublished data). In addition, the mutant *aip1-53* contains two mutations within the N-terminal propeller, Gly271Glu and Asp293Asn, which result in the loss of cofilin binding as well (Figures 1A and 2A). The unique aspect of this mutant is that it is the only allele that alters residues on the N-terminal propeller of Aip1p, with both mutations falling on blade 6. The necessity of the N-terminal propeller for the cofilin interaction is also supported by our preceding observation that the C-terminal propeller domain (residues 337–615), which has a weak two-hybrid interaction with actin, cannot interact with cofilin (as was also true for our gain-in-function C-terminal propeller mutations; Figure 2B). Therefore, these data collectively suggest that although cofilin largely contacts the C-terminal propeller of Aip1p, interactions with the N-terminal propeller are also essential to stabilize the interaction. All mutants and respective phenotypes addressed in this article are summarized in Table 3.

Molecular Docking of Aip1p and Cofilin

Molecular docking studies using Aip1p and cofilin resulted in a predicted complex between these two proteins. The complex shows impressive complementarity between the two protein surfaces considering that this is the result of docking simulations where both proteins were held rigid (Figure 3A). We have identified eight potential salt bridges that could be formed between the two proteins in this model and the residues involved are listed (cofilin residue–Aip1p residue): D123/E126-K533, E77-K89, D106-R18, D91-K410, R135-D585, R80-E111, K20-E136, and K82-D85. This model corresponds very well to the binding footprint predicted by our differential interaction screening, which identified Aip1p's cofilin binding domain (Figure 3B). In addition, biochemical evidence shows that cof1-19p is defective for Aip1p-induced actin filament disassembly (this work) and the mutated residues of this allele (R109, R110) are at the predicted Aip1p–cofilin interface. We also compared the docking results to three previously created mutant cofilin alleles, *cof1-4* (S4A), *cof1-13* (E59A, D61A), and *cof1-22* (E134A, R135A, R138A) (Lappalainen and Drubin, 1997), which have been shown to disrupt the interaction with Aip1p but not actin in the yeast two-hybrid system (Rodal *et al*., 1999). The *cof1-4* and *cof1-22* mutations lie at the predicted interface of the Aip1p–cofilin interaction in agreement with our model, whereas the *cof1-13* mutations face the opposite side of the cofilin molecule (Figure 3B). Although the *cof1-13* allele does not fit well with our docking model, this discrepancy may be explained by the fact that the mutated residues lie directly above several basic residues that are at the binding interface and may be disrupting the interaction through conformational/allosteric changes. Furthermore, based on the spacial disparity among the three mutant cofilin alleles implicated in the Aip1p interaction, it does not seem possible that a single molecular docking model can satisfy all three constraints.

Biochemical Analysis of Actin Filament Disassembly by aip1p Mutants

The following aip1p mutants that showed a defect by two-hybrid analysis were overexpressed in yeast as GST fusions and purified: aip1-15p, aip1-34/35p, aip1-55p, aip1-59p, aip1-60p (as a full-length version) as well as Aip1p WT. All aip1p mutants were then cleaved from GST by a thrombin digest, with the exception of aip1-15p, which we were unable to cleave. Our findings as well as those documented by Mohri *et al*. (2004) confirm that Aip1p-GST performs equally well as Aip1p in control disassembly assays. Each aip1p mutant was used in a severing assay, as described by Rodal *et al*. (1999). Although we are not positive that severing is the primary function being measured, we feel very strongly that this is the case and thus refer to these disassembly assays as severing assays. Briefly, 2.5 μM F-actin was combined with cofilin and Aip1p at a ratio of 20:20:1, respectively, and allowed to incubate at room temperature for 10 min. Samples were centrifuged at high speed (360,000 $\times$ *g*), and the efficiency of actin filament disassembly was measured by observing the pellet and supernatant fractions by SDS-PAGE. All of our severing assays showed that the aip1p mutants bound normally to the cofilin-decorated actin filaments, as observed by the amount of aip1p that pelleted with the remaining F-actin (our unpublished data). This indicates that none of the mutants were defective for F-actin binding in vitro. Only aip1-15p had a detectable severing defect, with a decrease in efficiency of ~50% (Figure 4, lane 3 versus lane 4). Based on our data, the N-terminal propeller's interaction with actin is far stronger in the two-hybrid system than the C-terminal propeller (Figure 2, A and B). These two-hybrid findings coupled with our biochemical data suggest that the Aip1p N-terminal propeller has a greater role than the C-terminal propeller for in vitro actin filament disassembly.

Table 3. Summary of the phenotypic analyses of *aip1* and *cof1* mutants

Allele	Mutations	Cell morphology	Two hybrid		Localization		Actin organization	Biochemistry
			With actin	With cofilin	Aip1p	Cofilin		
AIP1		WT	+++	+++	Cortical patches	Cortical patches	++++	Normal
*aip1*Δ		WT	na	na	na	Catches and cables	+++	na
aip1-15	I245A, E246A, D247A, D248A, Q249A, E250A	WT	+	+	Cortical patches	Patches and cables	+++	F-Actin depolym. defects
aip1-34/35	K571A, R572A, K575A/D516A, E521A	1% Elongated buds	+++	+++	Cortical patches	Patches and cables	+++	Normal
aip1-15/34/35	See above	nd	−	−	nd	nd	nd	Normal
aip1-51	H338P, A579T	nd	++	−	nd	nd	nd	nd
aip1-52	T558P	nd	++	−	nd	nd	nd	nd
aip1-53	G271E, D293N	nd	++	−	nd	nd	nd	nd
aip1-55	G449D	WT	++	−	Cortical patches	Patches and cables	+++	Normal
aip1-56	W261Stop	nd	++	−	nd	nd	nd	nd
aip1-59	S492L	1% Elongated buds	++	−	Cytosolic	Patches and cables	+++	Normal
aip1 C-term	G337-E615	nd	±	−	nd	nd	nd	nd
aip1-60	G337-E615, E615K	WT	+	−	Cortical patches	Cortical patches	++++	Normal
aip1-61	G337-E615, F481L	nd	+	−	nd	nd	nd	nd
			With actin	With Aip1p	Aip1p	Cofilin		
COF1		WT	+++	+++	Cortical patches	Cortical patches	++++	Normal
cof1-4	S4A	Enlarged	+++	−	Cortical patches	Cortical patches	+	Capping defect
cof1-19	R109A, R110A	Slightly enlarged	++	++	Cytosolic	Cortical patches	++	Severing and capping defects
cof1-13	E59A, D61A	WT	+++	−	Cortical patches	Cortical patches	++++	nd
cof1-22	E134A, R135A, R138A	nd	++	−	Cortical patches	Cortical patches	−	F-Actin depolym.

depolym., depolymerization; na, not applicable; nd, no data; +++, WT growth; ++, moderate growth; +, weak growth; ±, very weak growth; −, no growth.

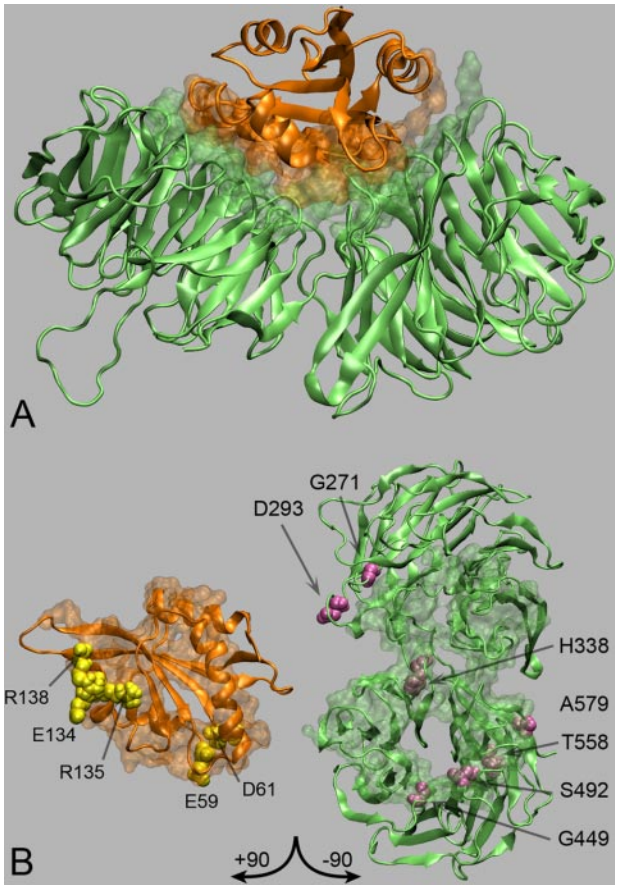

Figure 3. Molecular docking of the Aip1p–cofilin complex. (A) The predicted protein complex between Aip1p (green) and cofilin (orange) as the result of molecular docking studies. The contacting interfaces of the two proteins are rendered as a transparent surface to illustrate their complementarities. (B) The specific residues found to affect Aip1p–cofilin binding have been labeled and rendered as spheres. Yellow residues represent mutations that disrupt cofilin's two-hybrid interaction with Aip1p but not actin. Purple residues represent mutations that disrupt Aip1p's two-hybrid interaction with cofilin but not actin. This figure was created using VMD (Humphrey *et al*., 1996).

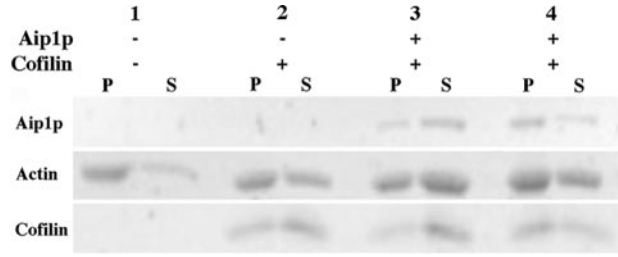

Figure 4. Biochemical analysis reveals a severing defect for the *aip1-15* mutation. Polymerized actin filaments (2.5 μM) were incubated with or without cofilin and GST-Aip1p (lane 3) or GST-aip1-15p (lane 4) for 10 min. The ratios of actin/cofilin and actin/Aip1p were 1:1 and 20:1, respectively. After high-speed centrifugation (360,000 $\times$ *g*), the extent of filament disassembly was determined based on the amount of actin that remained in the pellet fraction (F-actin) versus the supernatant fraction (G-actin), as detected by SDS-PAGE and SYPRO Ruby staining.

Biochemical Capping Analysis of Aip1p and Cof1p

We also intended to test our aip1p mutants using a biochemical actin filament-capping assay (Balcer *et al*., 2003). In this assay, F-actin is combined with profilin, cofilin, and Aip1p at a 20:40:4:1 ratio and allowed to incubate at room temperature for 20 min. Samples are then spun down at high speed (360,000 $\times$ *g*), and actin disassembly is assessed based on the amount of F-actin in the pellet versus the amount of actin in the supernatant. Theoretically, the cofilin concentration is too low for Aip1p to effectively bind and sever filaments (Rodal *et al*., 1999), but it should allow Aip1p to bind to barbed ends. As monomers dissociate from pointed ends, they form a dimeric complex with profilin, preventing them from rejoining at filament pointed ends but not at filament barbed ends. If Aip1p caps the barbed end of the actin filaments, the profilin-bound actin becomes sequestered, leading to a net depolymerization of the actin filaments from the pointed end.

We have observed a small but repeatable defect for cof1-19p in this assay, which is consistent with previous findings (Balcer *et al*., 2003). In addition, cof1-4p was found to have an even more severe defect (Figure 5 A, lanes 5–7). We also noticed that cof1-19p but not cof1-4 is defective in our severing assay (Figure 5A, lanes 2–4). Interestingly, when we repeated the capping assay using the cofilin mutants with and without Aip1p, the amount of actin disassembly looked nearly identical, indicating that in our hands this assay is not measuring Aip1p-related effects (compare Figure 5A, lanes 5–7 with Figure 5B, lanes 4–6). In an attempt to achieve Aip1p-dependent filament disassembly, we increased the actin concentration twofold (4 μM) and increased the profilin concentration 1.5-fold (6 μM), while leaving the cofilin and Aip1p concentrations the same (0.4 and 0.1 μM, respectively), thus increasing the actin:profilin:cofilin:Aip1p ratios to 40:60:4:1. The result was that disassembly no longer occurred without Aip1p, and subsequent addition of Aip1p to the reaction resulted in moderate filament disassembly (our unpublished data). However, we cannot be confident that this assay is in fact measuring barbed end capping rather than severing by Aip1p. Although the small amount of cofilin used in this experiment should not allow extensive Aip1p-induced severing, the cooperative nature of cofilin binding to filaments is likely to saturate short stretches of actin filaments (McGough *et al*., 1997; Ressad *et al*., 1998; Pope *et al*., 2000), creating ideal sites for Aip1p severing. We propose two scenarios of how minimal Aip1p-induced severing could lead to extensive disassembly of filaments in this assay. The first is that this assay is not measuring barbed-end regulation but is instead measuring the cumulative effects of cofilin-enhanced pointed-end disassembly plus monomer sequestration by profilin, which has been reported under some conditions (Carlsson *et al*., 1977). Aip1p-enhanced severing would create an increased number of short filaments that would not pellet during centrifugation, while also increasing the number of pointed ends from which filaments could disassemble, allowing profilin to more rapidly sequester the pool of actin in a monomeric state. Therefore, the cofilin mutant defects observed in this assay could simple be attributed to a decreased enhancement of pointed-end disassembly. The second explanation is that cofilin is having a profilin-dependent barbed-end gating effect, in which it blocks profilin-bound monomers from rejoining filaments at the barbed end. Severing by Aip1p would enhance the number of cofilin-decorated barbed ends, thus enhancing filament disassembly. Our F-actin plus profilin alone control sample (Figure 5B, lane 3) shows significant filament disassembly, most likely because of actin monomer

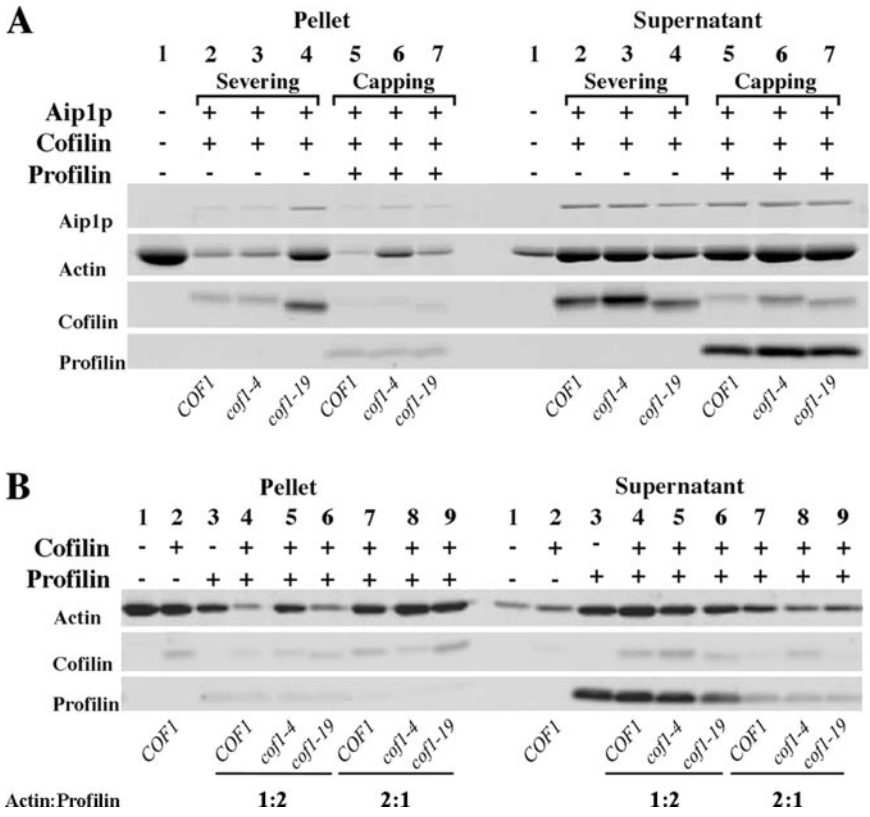

Figure 5. Biochemical capping assays demonstrate that cofilin-specific disassembly defects are Aip1p independent. In all cases, actin filament disassembly was measured by high-speed centrifugation (360,000 × *g*) followed by SDS-PAGE and SYPRO Ruby staining to compare the relative amounts of actin in the pellet (F-actin) versus actin in the supernatant (G-actin). (A) The cof1p mutants were tested for actin filament-severing and -capping defects in the presence of Aip1p. Polymerized actin filaments (2 μM) were incubated with or without cofilin, Aip1p, and profilin (where applicable). In lanes 2–4 (severing assay), the ratios of actin/cofilin and actin/Aip1p were 1:1 and 20:1, respectively. In lanes 5–7 (capping assay), the ratios of actin/cofilin, actin/Aip1p, and actin/profilin added were 5:1, 20:1, and 1:2, respectively. Lanes 2 and 5 contained wild-type cofilin. Lanes 3 and 6 contained cof1-4p. Lanes 4 and 7 contained cof1-19p. These data show that cof1-4p and cof1-19p have different defects depending on the method used to measure actin filament dynamics. (B) cof1p mutants were tested for actin filament-capping defects without Aip1p to determine whether the defects observed in 6A are Aip1p dependent. Polymerized actin filaments (2 μM) were incubated with or without cofilin and profilin. The actin/cofilin ratio is 5:1. The ratios for actin/profilin added were 1:2 (lanes 4–6) or 2:1 (lanes 7–9). Lanes 4 and 7 contained wild-type cofilin. Lanes 5 and 8 contained cof1-4p. Lanes 6 and 9 contained cof1-19p. These data show that under these conditions differences in assembly at the barbed end are Aip1p independent but cofilin dependent and differentially effected by cof1-4p versus cof1-19p. cof1-4p is more defective in the capping assay than cof1-19p, whereas cof1-19p is more defective than cof1-4p for Aip1p-induced severing.

sequestration by molar excess of profilin. In lanes 7–9, the profilin concentration is reduced to 25% of the previous level and filament disassembly is markedly reduced, compared with lanes 4–6. It is not clear whether this effect is strictly related to decreased monomer sequestration or whether this supports the idea of a cofilin-dependent barbed-end gating effect, because there are fewer profilin-bound actin monomers in these samples. The very limited degree to which cofilin alone is able to disassemble actin filaments hints at a synergistic effect with profilin, which would favor the gating hypothesis. In other words, even the total loss of the limited filament disassembly caused by cofilin alone (Figure 5B, compare lanes 1 and 2) does not seem as though it would be sufficient to account for the differences between the wild-type and mutant cofilins when they are combined with profilin (Figure 5B, lanes 4–6).

In summary, cof1p-associated defects in the capping assay persist in the absence of Aip1p and are thus unrelated to barbed-end capping by Aip1p. In addition, Aip1p-dependent filament disassembly was only achieved at increased actin concentrations, and this disassembly does not differentiate between actin filament severing and capping.

Genetic Analysis of aip1p Mutants

Despite the significant insights that have been made regarding Aip1p's ability to induce disassembly of cofilin-decorated actin filaments, the physiological role for these activities of Aip1p in yeast cortical actin patches has yet to be defined, and the relevance of Aip1p's reported filament-severing versus filament-capping activities remain a topic of debate. To begin to address these issues, we conducted a genetic screen in which we crossed an *aip1*Δ strain by a subarray of strains from the EUROSCARF nonessential gene deletion collection in *S. cerevisiae*. Each member of the subarray (listed in Table 4) was deleted for a gene whose product is known to encode a protein that localizes to cortical actin patches or is known to be involved in endocytosis (Balakrishnan *et al*., 2005). Because *aip1*Δ strains have fairly normal growth rates (Rodal *et al*., 1999), our goal was to identify synthetic growth defects in the double mutant strains, which would imply that the deleted subarray protein and Aip1p act in a common pathway or activity in the cell. Yeast strain MCY60 (*aip1*Δ*::NAT*^{r}) was mated to each of 74 deletion strains (*gene*Δ*::G418*^{r}), and diploids were selected, sporulated, tetrads were dissected, and genotyping was conducted to verify that any observed phenotypic abnormalities cosegregated with a double gene-deletion genotype. Of the 74 knockout alleles tested, only six were found to exhibit a synthetic slow-growth phenotype with the *aip1*Δ allele at 30°C: *sac6*Δ, *sla1*Δ, *rvs161*Δ, *rvs167*Δ, *cap1*Δ, and *cap2*Δ. We have previously reported the interactions between *aip1*Δ and *sac6*Δ, *sla1*Δ, *cap1*Δ, and *cap2*Δ (Rodal *et al*., 1999). However, this is the first exhaustive test for genetic interactions between all genes encoding components of the cortical patch and *AIP1*. The failure to see interactions between *aip1*Δ and the other 68 cortical patch/endocytosis genes tested suggests that Aip1p does not directly cooperate or act in concert with these other proteins or that some of these genes have redundant functions with one another, making it difficult to uncover *aip1*Δ interactions. As for the

Table 4. Genes tested for genetic interactions with *AIP1*

Gene name	ORF	Gene name	ORF	Gene name	ORF
LSB 6	YJL100w	ENT2	YLR206w	SRV2	YNL138w
DNM1	YLL001w	**SLA1**	YBL007c	TPM1	YNL079c
ENT4	YLL038c	EDE1	YBL047c	YPT53	YNL093w
APP2/GYL1	YMR192w	EDS1	YBR033w	INP52	YNL106c
INP53	YOR109w	LSB5	YCL034w	HUA1	YGR268c
SHE4/DIM1	YOR035c	ENT1	YDL161w	YAP1802	YGR241c
CLA4	YNL298w	**RVS161**	YCR009c	TVP18	YMR071c
MON2	YNL297c	RGD1	YBR260c	YCK3	YER123w
YCK2	YNL154c	AKR1	YDR264c	CRN1	YLR429w
VPS21	YOR089c	BRE4	YDL231c	LSB4/YSC84	YHR016c
HUA2	YOR284w	**SAC6**	YDR129c	NPL6	YMR091c
SCP1	YOR367w	SWA2	YDR320c	AIP1	YMR092c
YHL017w	YHL017w	PKH1	YDR490c	SVP26	YHR181w
INP51	YIL002c	MST27	YGL051w	SKM1	YOL113w
CAP2	YIL034c	**RVS167**	YDR388w	MYO3	YKL129c
TPM2	YIL138c	GTS1	YGL181w	SNO1	YMR095c
BZZ1	YHR114w	CHC1	YGL206c	MYO5	YMR109w
YIR003w	YIR003w	LSB1	YGR136w	LSB 3	YFR024c-A
YCK1	YHR135c	YAP1801	YHR161c	VRP1	YLR337c
PRK1	YIL095w	CLC1	YGR167w	ARK1	YNL020c
DID4	YKL002w	TWF1	YGR080w	YPT52	YKR014c
CAP1	YKL007w	BBC1/MTI1	YJL020c	APL4	YPR029c
APP1	YNL094w	ARC18	YLR370c	LSB2/PIN3	YPR154w
END3	YNL084c	SYP1	YCR030c	BSP1	YPR171w
SMY2	YBR172c	ABP1	YCR088w		

ORF, open reading frame. Bold text indicates a gene that shares a genetic interaction with *AIP1*.

six genes that did show an interaction with *aip1*Δ, all are involved in actin-related roles in the cell, are bona fide actin binding proteins, and are specifically linked to the vesicle internalization step of endocytosis (Engqvist-Goldstein and Drubin, 2003; Kaksonen *et al*., 2005). This is not surprising, because cortical actin patches have recently been proven to be early endocytic structures (Kaksonen *et al*., 2003; Huckaba *et al*., 2004; Rodal *et al*., 2005). The significance of these interactions is bolstered by the fact that Rvs161p and Rvs167p dimerize and are partially redundant for function (Lombardi and Riezman, 2001), whereas Cap1p and Cap2p dimerize to form the α/β heterodimeric actin filament barbed-end capping protein (Amatruda *et al*., 1990). Furthermore, these genes display extensive physical and genetic interactions among themselves (Balakrishnan *et al*., 2005; Figure 6). The synthetic genetic interactions between *aip1*Δ and the six cortical patch/endocytosis genes suggest an important physiological role for Aip1p in yeast cortical actin patches and the early steps of endocytosis. Also in support of these findings, *aip1* null mutants in *Dictyostelium* demonstrate reduced rates of endocytosis (Konzok *et al*., 1999). Additional assays will be necessary to determine the precise activities in which Aip1p is involved.

Genetic Interactions With aip1 Mutants Confirm Active Sites on the Aip1p Surface

To examine the relevance of Aip1p interactions to in vivo function, we crossed five *aip1* mutant strains, *aip1-15*, *aip1-34/35*, *aip1-55*, *aip1-59*, and *aip1-60* to *sac6*Δ, *sla1*Δ, *rvs161*Δ, *rvs167*Δ, *cap1*Δ, *cap2*Δ, and *cof1-4* strains to identify in vivo synthetic growth defects (Table 5). Interestingly, unlike with the *aip1*Δ allele, these double mutant strains had to be grown at 37°C rather than 30°C to detect any growth defects, indicating that our aip1p mutants are at least partially functional at 30°C. Only when crossed against the *cof1-4* strains did the *aip1* mutants mimic the phenotype of an *aip1*Δ allele at 30°C. We were unable to examine *aip1* crosses with *sac6*Δ or *sla1*Δ at 37°C, because both genes are essential at this temperature. *aip1-60*, which carries a gain-in-function mutation that enhances two-hybrid interaction with actin (see above; Figure 2B), was also tested in the context of full-length Aip1p and demonstrated a slow growth phenotype with *cof1-4* (Table 5).

Each of the four loss-of-function *aip1p* mutants tested in vivo showed significant synthetic growth defects when com-

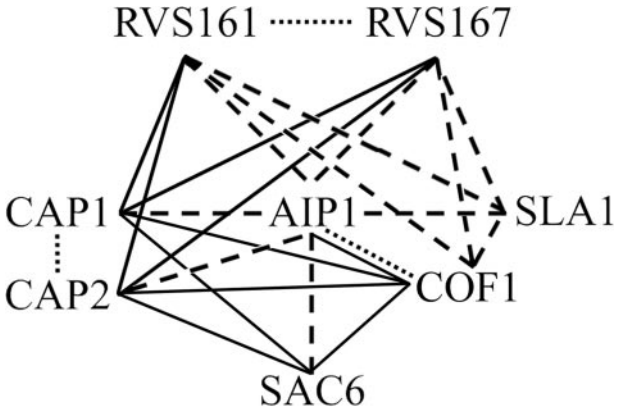

Figure 6. Physical and genetic interactions among cortical patch-localized genes and gene products. Dotted lines represent physical interactions between gene products. Dashed lines represent synthetic sick genetic interactions between null alleles or site-directed mutant alleles (cofilin). Solid lines represent synthetic lethal genetic interactions. Data obtained from the *S. cerevisiae* Genome Database (Balakrishnan, 2005) and this work.

Table 5. Summary of genetic interactions uncovered in this study

	AIP1	*aip1Δ*	*aip1-15*	*aip1-34/35*	*aip1-55*	*aip1-59*	*aip1-60*	*cof1-4*	*cof1-19*
30°C									
sac6Δ	+++	++	+++	+++	+++	+++	++++	+	++
sla1Δ	++++	+++	++++	++++	++++	++++	++++	+	+++
rvs161Δ	++++	+++	++++	++++	++++	++++	++++	++	++++
rvs167Δ	++++	+++	++++	++++	++++	++++	++++	++	++++
cap1Δ	++++	+++	++++	++++	++++	++++	++++	−	+
cap2Δ	++++	+++	++++	++++	++++	++++	++++	−	++
cof1-4	++++	−	−	−	−	−	++	na	na
cof1-19	++++	++++	nt	nt	nt	nt	++++	na	na
37°C									
sac6Δ	−	−	−	−	−	−	−	−	−
sla1Δ	−	−	−	−	−	−	−	−	−
rvs161Δ	+++	+	+	++	+++	+	++++	−	++
rvs167Δ	++	−	+	+	+	+	++++	+	++
cap1Δ	+++	+	++	++	+	+	++++	−	−
cap2Δ	+++	+	++	++	+	+	++++	−	−
cof1-4	+++	−	−	−	−	−	++	na	na
cof1-19	++++	++++	nt	nt	nt	nt	++++	na	na

nt, not tested; na, not applicable; ++++, WT growth; +++, moderate growth; ++, slow growth; +, very slow growth; −, dead.

bined with the endocytosis-related gene deletion strains (Table 5). In many cases, the intensity of these defects varied depending on the deletion strain being tested. Only one cross, *aip1-55* × *rvs161Δ*, failed to show a genetic interaction. As a whole, these findings show that both individual actin binding sites and the cofilin binding site are necessary for proper Aip1p activity in vivo.

If Aip1p is truly a barbed-end capping protein as reported previously (Okada *et al*., 2002; Balcer *et al*., 2003), we would expect the *aip1* mutants to have more serious synthetic defects with the *capΔ* alleles, because they would be expected to be redundant in function. Interestingly, the actin binding site-specific *aip1* alleles are more defective with the *rvs161/167* deletions than they are with the *cap1/cap2* deletions, suggesting a greater functional involvement of Aip1p and possibly Aip1p-facilitated severing with the RVS proteins than with the Cap proteins.

The *cof1-4* and *cof1-19* mutant alleles were also tested in combination with each *aip1* mutant allele and the six endocytosis-related gene deletions (Table 5). In all cases, *cof1-4* was more sick than *cof1-19*, suggesting that *cof1-4* defects which seem to be related to on/off rates at filament ends are of greater functional significance during this stage of endocytosis than the Aip1p-associated severing defect of *cof1-19*.

In addition to the synthetic growth defects describe above, haploid strains carrying each of the *aip1* mutants displayed various defects in cell morphology, actin organization, aip1p localization, and/or cofilin localization (Table 3 and Supplemental Figures S1–S3).

DISCUSSION

Mutagenesis and Computerized Docking Studies Predict a Model for the Actin–Cofilin–Aip1p Ternary Complex

Consistent with previously reported results (Mohri *et al*., 2004), we have identified an actin interaction site on Aip1p that seems to centralize along the outer rim of the N-terminal β-propeller. An incomplete loss of Aip1p function upon mutagenesis of this region led us to hypothesize that a second actin interacting site may exist on the C-terminal propeller, located analogously to the actin binding site of the N-terminal propeller. Several layers of genetic data support this proposition. First, a truncation mutant of Aip1p expressing only the C-terminal propeller shows a weak but consistent actin interaction in two-hybrid assays. Second, the suspected region for the actin interaction on this propeller was confirmed using site-directed loss-of-function mutations (alleles 34 and 35) as well as unbiased gain-in-function mutations (alleles 60 and 61). Third, when *aip1-34/35* and *aip1-60* mutants were integrated into the yeast genome in the context of the full-length Aip1p gene, both showed synthetic growth defects when combined with the *cof1-4* allele. *aip1-34/35* is also synthetic sick with a group of genes encoding endocytosis-related proteins.

Our random mutagenesis approach also identified a number of *aip1* mutants that are able to interact with actin but not cofilin in the two-hybrid system, revealing a cofilin-binding footprint along the front, concave surface of the molecule with essential contact points on the N- and C-terminal propellers. Each cofilin-specific mutant tested was also shown to have synthetic growth defects with *cof1-4* and genes encoding cortical patch proteins.

The active sites on Aip1p that we have identified are highly consistent with a molecular model acquired through independently conducted computerized docking studies of the Aip1p–cofilin complex. The cofilin-specific Aip1p mutations map extremely well to the Aip1p surface area that is buried by cofilin in the model. In agreement, cofilin mutants that have lost their ability to interact with Aip1p by two-hybrid (Rodal *et al*., 1999) are mostly consistent with the Aip1p binding interface on cofilin predicted by our model. Also of great significance is the fact that the cofilin residues mutated in the *cof1-19* (R109, R110) allele, which we have demonstrated to be deficient in vitro for Aip1p-induced actin filament severing, are at the predicted molecular interface with Aip1p. In addition, this model indicates that the regions of cofilin and Aip1p thought to be involved in actin binding are available and reasonably positioned for these interactions to occur. The actin and cofilin binding footprints seem to indicate a simple model for lateral actin filament binding by Aip1p in which it straddles cofilin while potentially binding two adjacent actin monomers. Observations

made by Mohri *et al*. (2004) support this model, because they showed that a *C. elegans* aip1p (unc-78) mutant capable of binding but not disassembling cofilin-decorated actin filaments reaches its filament binding saturation at a 2:1 actin-to-Aip1p ratio. Since actin has only one known Aip1p binding site and each Aip1p molecule has two actin binding sites, these data are consistent with the proposal that one molecule of Aip1p binds per two actin subunits within a filament. Furthermore, lateral filament binding by Aip1p has also been demonstrated by electron microscopy (Okada *et al*., 2002). Still, it remains unclear how Aip1p interacts with actin as a part of this complex. Specifically, we do not know whether both actin interacting sites bind to the actin filament simultaneously or whether one is used over the other under varying circumstances. Our experimental data suggest that both sites are important for optimal Aip1p function. In addition, how this leads to filament disassembly will require further investigation. We predict that Aip1p binding to cofilin-decorated actin filaments produces a torque that enhances the filament twist maintained by cofilin, leading to filament severing. Alternately, Aip1p may push cofilin deeper between subunits, wedging the filament apart by creating a steric hindrance between longitudinally associated actin monomers. In either case, we expect that significant conformational changes of the ternary complex occur immediately after Aip1p binding, which may cause difficulties in precisely predicting how this complex fits together. Our mutagenesis and modeling data coupled with the demonstrated ability of Aip1p to enhance the disassembly of cofilin-bound actin filaments (Rodal *et al*., 1999), and visual assays of tethered actin filaments treated with cofilin and Aip1p (Ono *et al*., 2004), strongly implicate Aip1p as an actin filament severing protein.

The inability of our aip1p mutants, with the exception of GST-aip1-15p, to show defects in a severing assay, although perplexing, is consistent with data from Mohri *et al*. (2004). Using *C. elegans* Aip1p (UNC-78), they were able to isolate N-terminal but not C-terminal propeller mutants (of four tested) that were defective in actin filament disassembly. Perhaps Aip1p-induced severing of actin filaments is so robust that more extreme mutational changes on the C-terminal propeller are necessary to obtain a biochemical defect. Consistent with this idea, we found that even while using minimal time periods of incubation and attempting to slow the rate of disassembly by conducting the experiments at 4°C, our severing reactions still proceeded to completion.

Is Aip1p a Capping Protein?

The biochemical activities of Aip1p from multiple sources (*S. cerevisiae*, *X. laevis*, and *C. elegans*) have been extensively tested in vitro (Okada *et al*., 1999, 2002; Rodal *et al*., 1999; Balcer *et al*., 2003; Mohri and Ono, 2003; Mohri *et al*., 2004; Ono *et al*., 2004). In actin pelleting assays, *S. cerevisiae* Aip1p very strongly induces the disassembly of cofilin-bound actin filaments, whereas *C. elegans* Aip1p (UNC-78) does so moderately, and *X. laevis* Aip1p (XAip1) does so very weakly (Okada *et al*., 1999; Rodal *et al*., 1999; Mohri and Ono, 2003). Although these disparities may be specific to the organism from which the Aip1p is obtained, it is possible that the weaker activities observed for UNC-78 and XAip1 have resulted from the use of rabbit skeletal muscle actin in the disassembly assays, whereas yeast Aip1p was tested using yeast actin. The ability of Aip1p to enhance severing of cofilin-decorated actin filaments has been convincingly documented (Okada *et al*., 1999; Ono *et al*., 2004). In addition, some findings indicate that Aip1p is able to cap the barbed ends of actin filaments, preventing filament elongation and thus enhancing disassembly (Okada *et al*., 2002; Balcer *et al*., 2003). Previous actin filament elongation assays using a range of XAip1 concentrations combined with cofilin provided persuasive evidence that XAip1 may exert a barbed-end capping activity (Okada *et al*., 2002). However, we have reservations regarding the biological relevance of this result because of the variety of sources from which reagents were obtained: rabbit muscle actin, chicken cofilin, and XAip1. In addition, an experiment suggesting that XAip1 is functionally redundant with the barbed-end capping gelsolin–actin complex used an actin/cofilin ratio of 27.5:1, which is far too low of a cofilin concentration for any expected Aip1p-associated disassembly and is thus inconclusive (Rodal *et al*., 1999; Okada *et al*., 2002). Visual assays of tethered actin filaments tested with UNC-78 were not able to confirm barbed-end capping of actin filaments by Aip1p at the concentrations tested and instead favored filament severing (Ono *et al*., 2004).

For *S. cerevisiae* Aip1p, we have demonstrated that capping assay defects associated with cof1-4p and cof1-19p persist in the absence of Aip1p, suggesting that Aip1p is not involved in the barbed-end activity that this assay was thought to measure. When we performed the capping assays using increased actin concentrations and lower respective profilin/cofilin/Aip1p ratios, Aip1p became necessary for filament disassembly, resulting in a moderate shift of actin from the pellet to the supernatant fraction. However, we are not convinced that these results represent barbed-end capping as opposed to severing for reasons described previously. Therefore, additional studies are necessary to further investigate barbed-end capping and to investigate the nature of possible concentration and/or species specificities associated with this activity.

Interestingly, in our actin disassembly assays we observed that cof1-4p is more defective in the capping assay while cof1-19p is more defective in the severing assay, indicating that cofilin is playing a different role in each of these two assays. Cofilin's role in the capping assay seems to be profilin related, although it is not clear whether enhanced actin filament disassembly is caused by additive profilin/cofilin effects or synergistic effects caused by profilactin-specific barbed-end gating by cofilin. Approximations for the concentrations of actin and profilin in yeast are 60 and 20 μM, respectively (Magdolen *et al*., 1993). Presuming that the F-actin/G-actin ratio in yeast is at least 1:1, as has been stated for other organisms (Korn, 1982; Hug *et al*., 1995), then the G-actin/profilin ratio would be expected to be ~3:2. Therefore, because the majority of actin monomers within the cell could be profilin bound, cofilin gating of barbed ends is a feasible hypothesis for a novel mode of barbed-end regulation.

If Aip1p were not involved in barbed-end capping, that would leave filament severing as Aip1p's only recognized role in the cell. Therefore, it seems paradoxical that an *aip1*Δ strain is SL with *cof1-4*, which may be defective in barbed-end regulation but not in severing assays, whereas it is not SL with *cof1-19*, which shows considerable Aip1p-induced severing defects. Our proposed potential barbed-end regulating activity for cofilin, if verified, might explain this observation. It may be that a primary role of Aip1p is to create cofilin-decorated barbed ends through severing. On the other hand, Aip1p severing would also create more cofilin-decorated pointed ends, potentially enhancing filament disassembly by subunit release from this end of the filament. Furthermore, cofilin-bound filament ends could differ drastically from bare ends in terms of growth kinetics and in the ability to interact with other filament end-associated proteins, such as capping proteins, formins, and the Arp2/3 complex.

Aip1p capping and profilactin gating by cofilin could both occur at actin filament barbed ends, with local protein concentrations being a deciding factor as to which activity prevails. Therefore, additional visual and kinetic biochemical assays are necessary to conclusively differentiate between severing, capping, and gating of actin filaments. If Aip1p is involved with the regulation of filament barbed ends, it would likely act in a cooperative manner with the filament severing activity: Aip1p induces actin filament severing at its site of lateral filament binding, then remains bound to the newly created barbed end where it may participate in blocking subunit addition. Thus, severing could serve as a way for Aip1p to self-target to filament barbed ends. Electron microscopy in conjunction with molecular docking studies may provide details regarding the precise mechanisms by which Aip1p induces cofilin-mediated actin filament disassembly.

Genetic Interactions Reveal That Aip1p Plays a Role in Endocytosis in Yeast

During the process of endocytosis in yeast, Rvs161p and Rvs167p have been implicated in linking actin to the neck of the invaginated vesicle, where all three proteins contribute to vesicular scission (Schmidt *et al*., 1999; Baggett and Wendland, 2001; Jeng and Welch, 2001). Sla1p is known to be involved with organization and assembly of actin networks within cortical patches and a *sla1*Δ strain has large, flattened cortical patches and endocytic defects (Rodal *et al*., 1999; Warren *et al*., 2002). Sac6p (fimbrin) is an actin filament bundling protein that forms parallel cross-links between actin filaments (Bretscher, 1981). Cap1p and Cap2p form a heterodimeric complex that caps the barbed ends of actin filaments (Amatruda *et al*., 1992). All six of these proteins have been directly linked to vesicle internalization in yeast (Kaksonen *et al*., 2005). The slow growth phenotypes observed when *aip1*Δ is combined with these gene deletions but not with dozens of other deletions of cortical patch genes point to a direct role for Aip1p in endocytic vesicle internalization.

Cytological Observation of aip1 Mutant Strains Expose In Vivo Defects

Consistent with our genetic findings, we were able to visually observe morphological aberrations within our *aip1* mutant strains using fluorescent microscopy. Actin organizational defects at least partially similar to an *aip1*Δ strain were seen in all mutant strains except for *aip1-60* (Supplemental Figure S1). Interestingly, *aip1-34/35* and *aip1-59* also displayed elongated buds in 1–2% of the cells observed. We have never observed this novel phenotype in WT or *aip1*Δ strains, suggesting that the presence of impaired aip1p has the potential to be more functionally detrimental to the cell than the elimination of Aip1p all together. This is likely the result of some partial obstruction of Aip1p and/or cofilin activity that leads to an imbalance in actin filament growth dynamics.

Immunofluorescence of aip1p in the mutant strains also showed deviations from normal, ranging from a slight decrease to a total loss of cortical patch localization for the loss of function mutants, whereas aip1-60p demonstrated an enhanced localization at cortical patches (Supplemental Figure S2). Only aip1-34/35p did not have any observable mislocalization.

Cofilin localization was also performed in our aip1p mutant strains (Supplemental Figure S3). In an *aip1*Δ strain, cofilin partially mislocalizes to the cytoplasm where it exists in a filamentous state, presumably decorating cellular actin cables. Of the mutants tested, only *aip1-60* did not at least partially mimic this phenotype. However, *aip1-60* did enhance the cytoplasmic cofilin localization of the *cof1-19* strain. The accumulation of cofilin-decorated cables in the cytoplasm of *aip1* and *cof1* strains suggest that the roles played by these proteins are not limited to actin cortical patches and that they likely act in cytoplasmic cable disassembly, perhaps by clearing excess filaments out of the cytoplasm. Furthermore, the fact that our mutants partially imitate an *aip1*Δ phenotype bolsters the physiological relevance of the active sites that we have identified on Aip1p.

The complexities of the cooperative activities conducted by Aip1p, cofilin, and possibly profilin extend beyond these proteins to include regulatory factors as well. Because of the intensely robust ability that Aip1p and cofilin have to disassemble actin filaments, as demonstrated by in vitro biochemical assays, cellular mechanisms must exist that prevent these proteins from uncontrollably shredding filaments in vivo. Were this not the case, Aip1p and cofilin would not colocalize with actin filaments in cortical patches. Thus, considerable progress remains to be made in further elucidating the precise activities of Aip1p and cofilin in vivo and in evaluating how these functions are regulated and balanced to enhance the dynamics of actin networks.

ACKNOWLEDGMENTS

We thank B. Goode, K. Okada, S. Ono, and K. Mohri for sharing unpublished data and constructive suggestions. We also thank T. Duncan for assistance with molecular modeling programs to create figures and all members of the Amberg laboratory for helpful input. This research was supported by National Institutes of Health Grants GM-067246 (to D. S.) and GM-56189 (to D.C.A.).

REFERENCES

Amatruda, J. F., Cannon, J. F., Tatchell, K., Hug, C., and Cooper, J. A. (1990). Disruption of the actin cytoskeleton in yeast capping protein mutants. Nature *344*, 352–354.

Amatruda, J. F., Gattermeir, D. J., Karpova, T. S., and Cooper, J. A. (1992). Effects of null mutations and overexpression of capping protein on morphogenesis, actin distribution and polarized secretion in yeast. J. Cell Biol. *119*, 1151–1162.

Amberg, D. C., Basart, E., and Botstein, D. (1995). Defining protein interactions with yeast actin *in vivo*. Nat. Struct. Biol. *2*, 28–35.

Amberg, D. C., Burke, D. J., and Strathern, J. N. (2005). Methods in Yeast Genetics: A Cold Spring Harbor Laboratory Course Manual, Cold Spring Harbor, NY: Cold Spring Harbor Laboratory Press.

Baggett, J. J., and Wendland, B. (2001). Clathrin function in yeast endocytosis. Traffic *2*, 297–302.

Balakrishnan, R., *et al*. (2005). Saccharomyces Genome Database. http://www.yeastgenome.org/ (accessed 23 December 2005).

Balcer, H. I., Goodman, A. L., Rodal, A. A., Smith, E., Kugler, J., Heuser, J. E., and Goode, B. L. (2003). Coordinated regulation of actin filament turnover by a high-molecular-weight Srv2/CAP complex, cofilin, profilin, and Aip1. Curr. Biol. *13*, 2159–2169.

Bobkov, A. A., Muhlrad, A., Kokabi, K., Vorobiev, S., Almo, S. C., and Reisler, E. (2002). Structural effects of cofilin on longitudinal contacts in F-actin. J. Mol. Biol. *323*, 739–750.

Bretscher, A. (1981). Fimbrin is a cytoskeletal protein that crosslinks F-actin in vitro. Proc. Natl. Acad. Sci. USA *78*, 6849–6853.

Carlier, M. F., Laurent, V., Santolini, J., Melki, R., Didry, D., Xia, G. X., Hong, Y., Chua, N. H., and Pantaloni, D. (1997). Actin depolymerizing factor (ADF/cofilin) enhances the rate of filament turnover: implication in actin-based motility. J. Cell Biol. *136*, 1307–1322.

Carlsson, L., Nystrom, L. E., Sundkvist, I., Markey, F., and Lindberg, U. (1977). Actin polymerizability is influenced by profilin, a low molecular weight protein in non-muscle cells. J. Mol. Biol. *115*, 465–483.

Durfee, T., Becherer, K., Chen, P.-L., Yeh, S.-H., Yang, Y., Kilburn, A.E., Lee, W.-H., and Elledge, S. J. (1993). The retinoblastoma protein associates with the protein phosphatase type 1 catalytic subunit. Genes Dev. *7*, 555–569.

Engqvist-Goldstein, A. E., and Drubin, D. G. (2003). Actin assembly and endocytosis: from yeast to mammals. Annu. Rev. Cell Dev. Biol. *19*, 287–332.

Fields, S., and Song, O. (1989). A novel genetic system to detect protein-protein interactions. Nature *340*, 245–246.

Galkin, V. E., Orlova, A., VanLoock, M. S., Shvetsov, A., Reisler, E., and Egelman, E. H. (2003). ADF/cofilin use an intrinsic mode of F-actin instability to disrupt actin filaments. J. Cell Biol. *163*, 1057–1066.

Gerisch, G., Faix, J., Kohler, J., and Muller-Taubenberger, A. (2004). Actin-binding proteins required for reliable chromosome segregation in mitosis. Cell Motil. Cytoskeleton *57*, 18–25.

Haarer, B. K., Lillie, S. H., Adams, A.E.M., Magdolen, V., Bandlow, W., and Brown, S. S. (1990). Purification of profilin from *Saccharomyces cerevisiae* and analysis of profilin-deficient cells. J. Cell Biol. *110*, 105–114.

Huckaba, T. M., Gay, A. C., Pantalena, L. F., Yang, H. C., and Pon, L. A. (2004). Live cell imaging of the assembly, disassembly, and actin cable-dependent movement of endosomes and actin patches in the budding yeast, *Saccharomyces cerevisiae*. J. Cell Biol. *167*, 519–530.

Hug, C., Jay, P. Y., Reddy, I., McNally, J. G., Bridgman, P. C., Elson, E. L., and Cooper, J. A. (1995). Capping protein levels influence actin assembly and cell motility in *Dictyostelium*. Cell *81*, 591–600.

Humphrey, W., Dalke, A., and Schulten, K. (1996). VMD: visual molecular dynamics. J. Mol. Graph *14*, 27–28, 33–38.

Ichetovkin, I., Han, J., Pang, K. M., Knecht, D. A., and Condeelis, J. S. (2000). Actin filaments are severed by both native and recombinant *Dictyostelium* cofilin but to different extents. Cell Motil. Cytoskeleton *45*, 293–306.

Iida, K., and Yahara, I. (1999). Cooperation of two actin-binding proteins, cofilin and Aip1, in *Saccharomyces cerevisiae*. Genes to Cells *4*, 21–32.

Jacobson, M. P., Pincus, D. L., Rapp, C. S., Day, T. J., Honig, B., Shaw, D. E., and Friesner, R. A. (2004). A hierarchical approach to all-atom protein loop prediction. Proteins *55*, 351–367.

Jeng, R. L., and Welch, M. D. (2001). Cytoskeleton: actin and endocytosis–no longer the weakest link. Curr. Biol. *11*, R691–R694.

Kaksonen, M., Sun, Y., and Drubin, D. G. (2003). A pathway for association of receptors, adaptors, and actin during endocytic internalization. Cell *115*, 475–487.

Kaksonen, M., Toret, C. P., and Drubin, D. G. (2005). A modular design for the clathrin- and actin-mediated endocytosis machinery. Cell *123*, 305–320.

Kale, L.E.A. (1999). NAMD2: greater scalability for parallel molecular dynamics. J. Comput. Phys. *151*, 283–312.

Ketelaar, T., Allwood, E. G., Anthony, R., Voigt, B., Menzel, D., and Hussey, P. J. (2004). The actin-interacting protein AIP1 is essential for actin organization and plant development. Curr. Biol. *14*, 145–149.

Konzok, A., Weber, I., Simmeth, E., Hacker, U., Maniak, M., and Muller-Taubenberger, A. (1999). DAip1, a Dictyostelium homologue of the yeast actin-interacting protein 1, is involved in endocytosis, cytokinesis, and motility. J. Cell Biol. *146*, 453–464.

Korn, E. D. (1982). Actin polymerization and its regulation by proteins from nonmuscle cells. Physiol. Rev. *62*, 672–737.

Kron, S. J., Drubin, D. G., Botstein, D., and Spudich, J. A. (1992). Yeast actin filaments display ATP-dependent sliding movement over surfaces coated with rabbit muscle myosin. Proc. Natl. Acad. Sci. USA *89*, 4466–4470.

Lappalainen, P., and Drubin, D. G. (1997). Cofilin promotes rapid actin filament turnover *in vivo*. Nature *388*, 78–82.

Lombardi, R., and Riezman, H. (2001). Rvs161p and Rvs167p, the two yeast amphiphysin homologs, function together in vivo. J. Biol. Chem. *276*, 6016–6022.

Ma, H., Kunes, S., Schatz, P. J., and Botstein, D. (1987). Plasmid construction by homologous recombination in yeast. Gene *58*, 201–216.

Maciver, S. K., Zot, H. G., and Pollard, T. D. (1991). Characterization of actin filament severing by actophorin from *Acanthamoeba castellanii*. J. Cell Biol. *115*, 1611–1620.

Magdolen, V., Drubin, D. G., Mages, G., and Bandlow, W. (1993). High levels of profilin suppress the lethality caused by overproduction of actin in yeast cells. FEBS Lett. *316*, 41–47.

McGough, A., Pope, B., Chiu, W., and Weeds, A. (1997). Cofilin changes the twist of F-actin: implications for actin filament dynamics and cellular function. J. Cell Biol. *138*, 771–781.

Mohri, K., and Ono, S. (2003). Actin filament disassembling activity of *Caenorhabditis elegans* actin-interacting protein 1 (UNC-78) is dependent on filament binding by a specific ADF/cofilin isoform. J. Cell Sci. *116*, 4107–4118.

Mohri, K., Vorobiev, S., Fedorov, A. A., Almo, S. C., and Ono, S. (2004). Identification of functional residues on *Caenorhabditis elegans* actin-interacting protein 1 (UNC-78) for disassembly of actin depolymerizing factor/cofilin-bound actin filaments. J. Biol. Chem. *279*, 31697–31707.

Morris, G. M., Goodsell, D. S., Halliday, R. S., Huey, R., Hart, W. E., Belew, R. K., and Olson, A. J. (1998). Automated docking using a lamarckian genetic algorithm and empirical binding free energy function. J. Comput. Chem. *19*, 1639–1662.

Okada, K., Blanchoin, L., Abe, H., Chen, H., Pollard, T. D., and Bamburg, J. R. (2002). *Xenopus* actin interacting protein 1 (XAip1) enhances cofilin fragmentation of filaments by capping filament ends. J. Biol. Chem. *277*, 43011–43016.

Okada, K., Obinata, T., and Abe, H. (1999). XAIP1*:* a *Xenopus* homologue of yeast actin interacting protein 1 (AIP1), which induces disassembly of actin filaments cooperatively with ADF/cofilin family proteins. J. Cell Sci. *112*, 1553–1565.

Ono, S. (2001). The *Caenorhabditis elegans unc-78* gene encodes a homologue of actin-interacting protein 1 required for organized assembly of muscle actin filaments. J. Cell Biol. *152*, 1313–1319.

Ono, S., Mohri, K., and Ono, K. (2004). Microscopic evidence that actin-interacting protein 1 actively disassembles actin depolymerizing factor/cofilin-bound actin filaments. J. Biol. Chem. *279*, 14207–14212.

Pope, B. J., Gonsior, S. M., Yeoh, S., McGough, A., and Weeds, A. G. (2000). Uncoupling actin filament fragmentation by cofilin from increased subunit turnover. J. Mol. Biol. *298*, 649–661.

Ressad, F., Didry, D., Xia, G. X., Hong, Y., Chua, N. H., Pantaloni, D., and Carlier, M. F. (1998). Kinetic analysis of the interaction of actin-depolymerizing factor (ADF)/cofilin with G- and F-actins. Comparison of plant and human ADFs and effect of phosphorylation. J. Biol. Chem. *273*, 20894–20902.

Rodal, A. A., Kozubowski, L., Goode, B. L., Drubin, D. G., and Hartwig, J. H. (2005). Actin and septin ultrastructures at the budding yeast cell cortex. Mol. Biol. Cell *16*, 372–384.

Rodal, A. A., Tetreault, J. W., Lappalainen, P., Drubin, D. G., and Amberg, D. C. (1999). Aip1p interacts with cofilin to disassemble actin filaments. J. Cell Biol. *145*, 1251–1264.

Rogers, S. L., Wiedemann, U., Stuurman, N., and Vale, R. D. (2003). Molecular requirements for actin-based lamella formation in *Drosophila* S2 cells. J. Cell Biol. *162*, 1079–1088.

Rose, M. D., Winston, F., and Hieter, P. (1989). Methods in Yeast Genetics, Cold Spring Harbor, NY: Cold Spring Harbor Laboratory Press.

Schmidt, A., Wolde, M., Thiele, C., Fest, W., Kratzin, H., Podtelejnikov, A. V., Witke, W., Huttner, W. B., and Soling, H. D. (1999). Endophilin I mediates synaptic vesicle formation by transfer of arachidonate to lysophosphatidic acid. Nature *401*, 133–141.

Voegtli, W. C., Madrona, A. Y., and Wilson, D. K. (2003). The structure of Aip1p, a WD repeat protein that regulates cofilin-mediated actin depolymerization. J. Biol. Chem. *278*, 34373–34379.

Warren, D. T., Andrews, P. D., Gourlay, C. W., and Ayscough, K. R. (2002). Sla1p couples the yeast endocytic machinery to proteins regulating actin dynamics. J. Cell Sci. *115*, 1703–1715.

Wertman, K. F., Drubin, D. G., and Botstein, D. (1992). Systematic mutational analysis of the yeast *ACT1* gene. Genetics *132*, 337–350.